ELSEVIER

PII: S0266-3538(96)00110-8

*Composites Science and Technology* **57** (1997) 55–65

0266-3538/97/$17.00

# DYNAMIC CRACK INITIATION AND GROWTH IN THICK UNIDIRECTIONAL GRAPHITE/EPOXY PLATES

John Lambros[a] & Ares J. Rosakis[b]

[a]*Department of Mechanical Engineering, University of Delaware, Newark, Delaware 19716, USA*
[b]*Graduate Aeronautical Laboratories, California Institute of Technology, Pasadena, California 91125, USA*

(Received 4 April 1996; revised 19 July 1996; accepted 2 August 1996)

**Abstract**

*In this work we present some preliminary results of optical experiments performed on dynamically deforming thick polymeric-composite laminate plates. The composites used for this study are unidirectional graphite/epoxy fiber-reinforced composite plates, consisting of 48 plies (6 mm thickness). Edge-notched plates are impact loaded in a one-point bend configuration using a drop-weight tower. The lateral shearing interferometer of coherent gradient sensing (CGS), in conjunction with high-speed photography, is used to obtain real-time interferograms of the near-tip deformation during dynamic crack initiation and growth. Initiation fracture toughness data are obtained and reported. Crack growth speeds of 900 m s$^{-1}$ are recorded and significant dynamic effects are observed through emission of stress waves from the propagating crack tip.* © *1997 Elsevier Science Limited*

*Keywords:* dynamic crack initiation, unidirectional graphite/epoxy plates, crack growth

## 1 INTRODUCTION

Fiber-reinforced polymeric composite laminates have seen extensive use in the aircraft industry during the past few decades. They have consistently proved their capability for significant weight savings in aircraft and spacecraft structures. It is now proposed to use thick polymeric composite laminates in the construction of submersibles and other naval structures. With the growing use of composite materials in engineering applications, the need for fundamental understanding of their mechanical behavior becomes more compelling. Of primary importance, especially as regards integrity and safety of composite structures, is the complete understanding of all damage and failure processes that occur in composite materials. The term damage, as applied to composite materials, usually encompasses an array of possible events occurring over a range of length scales and dependent on the particular composite type (e.g. fiber or particle reinforcement, metal or ceramic matrix, etc.). For polymeric-matrix fiber-reinforced composite laminates failure modes include ply delamination, fiber/matrix debonding, fiber pull-out and matrix cracking. In many service situations damage and failure can occur in a dynamic fashion, usually triggered by some sudden structural overload (e.g. foreign-object impact). Even though in general a complicated combination of these damage modes will be responsible for failure of a service component, it is extremely difficult to investigate experimentally all failure modes simultaneously in real time in a laboratory situation. In the present work we isolate one of the many forms of failure. Here we concentrate on the experimental investigation of dynamic crack initiation and propagation in unidirectional fiber-reinforced polymeric-matrix composite plates.

Quasi-static fracture of composite materials is a subject which has been much investigated in the past few decades, both theoretically and experimentally (e.g. Prahizar *et al.*[1]). Several quasi-static fracture criteria have been proposed in the past (e.g. Tohgo *et al.*,[2] Binieda *et al.*[3]) for unidirectional composite laminates, and many experimental studies have been conducted in support of them. In addition, recently, Liu *et al.*[4] have investigated quasi-static fracture of polymeric composite laminates by using the optical technique of coherent gradient sensing (CGS). However, very little work has been done which involves the real-time investigation of dynamic fracture of composite materials. The little that has been done is primarily restricted to theoretical studies of crack propagation in orthotropic or anisotropic media, as for example the work of Tsai,[5] who studied the dynamic behavior of a crack in an orthotropic plate, or the work of Mannion and Pipkin,[6] who investigated cracks paths in fiber-reinforced composites by utilizing various postulated fracture criteria. In another example, theoretical predictions for the limiting crack tip speed in a unidirectional lamina were made in the work of Chiang.[7] To our knowledge, very few experimental studies of dynamic fracture of

fiber-reinforced composites have been performed. In the work of Shukla and Khanna[8] the authors were primarily concerned with the interaction of a matrix crack approaching the fibers in a fiber-reinforced brittle matrix, an event occurring at the composite microscale. Dealing with a different length-scale problem, Khanna and Shukla[9] recently obtained an expression for the most singular term of the stress and strain fields surrounding the tip of a crack growing dynamically in an orthotropic material. Using well-positioned strain gauges, they utilized their analytical result to obtain stress-intensity factor histories in laboratory tests.

To our knowledge, the only studies in which optical techniques and high-speed photography have been utilized to investigate damage in composites have dealt with real-time imaging of dynamic delamination and penetration in composites. Chai *et al.*[10] and Chai and Babcock,[11] using the shadow moiré technique, performed optical measurements on composites subjected to low-velocity out-of-plane impact. More recently Epstein *et al.*[12] used dynamic moiré interferometry to measure the deflection of impacted composite plates. Zhu *et al.*[13] photographed very-high-speed projectiles penetrating Kevlar laminates. Although the results of these studies are not directly related to the subject covered in the present paper, i.e. fracture of unidirectional composites, they do however provide evidence of the feasibility of performing real-time visualization of impact in composite materials.

The novelty of the research we are presently conducting is based on the *real-time* visualization of dynamic fracture initiation and growth in pre-cracked composite laminate plates subjected to in-plane, one-point bend impact loading. The optical method used for real-time visualization was the newly developed full-field optical method of coherent gradient sensing (CGS) in reflection.[14,15] Imaging was performed with a rotating-mirror high-speed camera. Our aim in this paper is to provide evidence of the feasibility of the use of CGS interferometry for imaging dynamic deformation and fracture of composite laminates and to visualize for the first time macroscopic dynamic crack growth in thick polymeric composite laminates subjected to impact loading.

## 2 DETAILS OF EXPERIMENTS

### 2.1 The optical method of CGS in reflection

Consider a planar wave front normally incident on an optically flat and specularily reflective surface of an opaque plate. The undeformed specimen surface occupies the $(x_1, x_2)$ plane (see Fig. 1). After impact the specimen surface deforms and acquires an out-of-plane displacement $u_3(x_1, x_2)$. Incident parallel rays reflected from the deformed specimen surface will deviate from parallelism after reflection. In this situation the reflected wave front will no longer be planar. The CGS set-up is used to provide full-field information about the amount of deviation from parallelism of each reflected ray. It is possible, as shown in detail in Rosakis,[15] to relate the resulting interferograms with either the slope or the difference of out-of-plane displacement $u_3$.

A schematic of the experimental apparatus is shown in Fig. 1. When the rays are reflected from the specimen, they are processed by a pair of high-density gratings, $G_1$ and $G_2$, separated a distance $\Delta$ apart (in these experiments typically 60 mm). In a typical set-up, the gratings have their rulings parallel to either the $x_1$ or $x_2$ direction. The grating pitch is denoted by $p$ which is equal to 0·0254 mm in these experiments (i.e. 40 lines/mm). The action of the gratings is to displace (shear) the reflected beam and recombine it with itself, thus creating an interferogram after $G_2$. The light emerging from $G_2$ is collected by a filtering lens L and its frequency content (diffraction spots) is

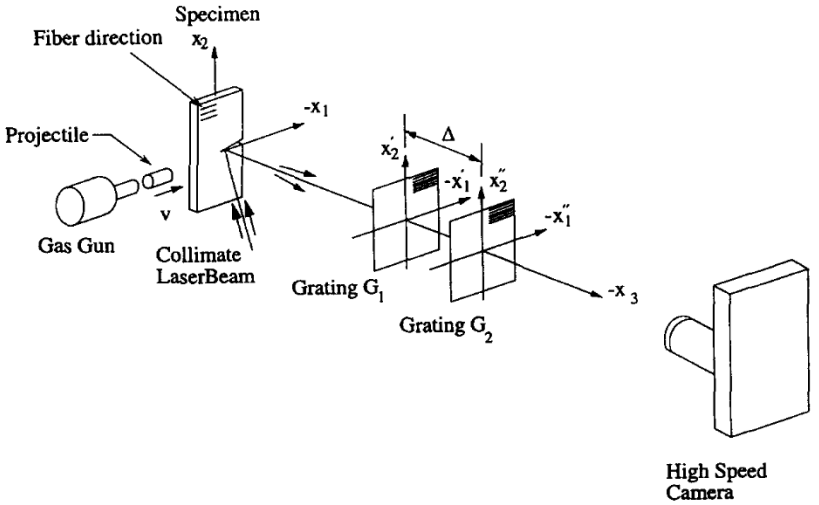


**Fig. 1.** Schematic illustration of CGS set-up in reflection for use in dynamic fracture experiments of composite materials.

displayed on the back focal plane. By locating a filtering aperture around either the ±1 diffraction orders, information regarding the change of out-of-plane displacement $u_3$ along either the $x_1$ or $x_2$ axis is obtained on the image plane.

As demonstrated by a first-order analysis described by Tippur *et al.*[14] or a higher order Fourier optics analysis by Lee *et al.*,[16] when the two diffraction gratings $G_1$ and $G_2$ are placed very close to each other (i.e. small $\Delta$) the resulting bright fringes can be related to *gradient components* of $u_3$ as follows:

$$\frac{\partial(u_3)}{\partial x_\alpha} = \frac{k_\alpha p}{2\Delta} \quad \alpha = (1,2) \tag{1}$$

where

$$k_\alpha = \begin{Bmatrix} m \text{ for } \alpha = 1,\ m = 0, \pm 1, \pm 2, \ldots \\ n \text{ for } \alpha = 2,\ n = 0, \pm 1, \pm 2, \ldots \end{Bmatrix}$$

and $m$ and $n$ are the fringe orders for the $x_1$, $x_2$ gradient contours, respectively. For grating rulings perpendicular to the $x_\alpha$ axis the resulting fringe pattern is proportional to $\partial(u_3)/\partial x_\alpha$, $\alpha = (1,2)$. For the case in which separation $\Delta$ becomes large compared with the angular deviation of the light rays, a difference rather than derivative approach must be used (see Bruck and Rosakis[17,18]). In such a case formation of constructive interference on the image plane is governed by:

$$\Delta u_3 = u_3\left(\boldsymbol{x} + \frac{\varepsilon}{2}\right) - u_3\left(\boldsymbol{x} - \frac{\varepsilon}{2}\right) = \frac{kp\varepsilon}{2\Delta}, \quad k\text{: integer} \tag{2}$$

where $\Delta u_3$ denotes the difference of $u_3$, $\boldsymbol{x}$ is the position vector of any point in the interference of the laser beams (as seen in Fig. 2). In eqn (2) $\varepsilon$ is the shearing distance (also shown in Fig. 2) and is easily evaluated from $\varepsilon \approx \Delta\lambda/p$, where $\lambda$ is the wavelength of light used. Since we do not expect a substantial $u_3$ during the deformation of the relatively brittle composite, a large $\Delta$ will be utilized so as to increase the sensitivity of the interferometer. Therefore all analysis performed in Section 3.2 will be based on a difference approach (i.e. eqn (2)).

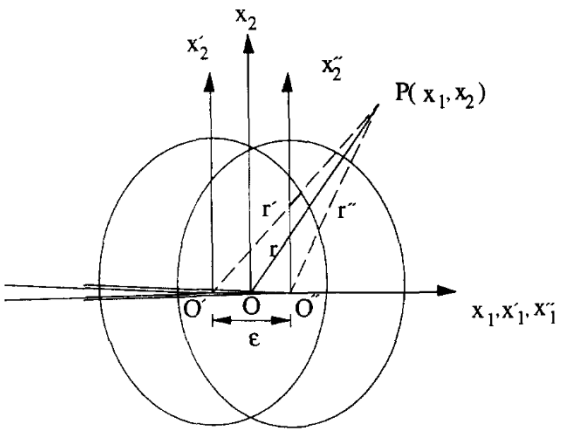


**Fig. 2.** Interpretation of interferograms by utilization of a difference approach for large beam shearing. Apparent crack tips are centered at O′ and O″.

### 2.2 Specimen preparation and characterization

The particular composite chosen for this study was a unidirectional graphite/epoxy system, with a fiber strength of 231 GPa ($33 \times 10^6$ psi) and a fiber volume fraction of 0·65. The in-plane dimensions of the plate specimens used were 76 mm × 152 mm (3 in × 6 in) or 101 mm × 152 mm (4 in × 6 in). The plates consisted of a total of 48 plies, resulting in a nominal thickness of 6 mm (0·25in). In all cases a precrack of length $0{\cdot}2W$ (where $W$ is the width of the plate) was machined in the center of the plate, parallel to the shorter side and along the fiber direction. A crack length of $0{\cdot}2W$ was used because this has been seen in the past to produce reliable results in dynamic fracture experiments in homogeneous materials.[19] To minimize residual cutting stresses a low-speed diamond saw was used to generate the precrack. Precracks resulting from this procedure had a notch width of approximately 1·5 mm. In certain cases a sharper precrack was introduced by extending the diamond saw notch with a sharp razor blade. Results will be presented for both the case of a sharp precrack and a blunt notch.

In order to perform interferometric experiments on opaque composite plates at least one surface must be optically flat and specularily reflective. Such a surface was achieved by applying an extra layer of resin on one side of the composite plate before cure. Subsequent curing of the composite under pressure against an optically flat tool (a thick glass substrate) resulted in an optically flat surface. The optically flat composite plates were provided by Composite Mirror Applications Inc. of Tucson, Arizona. To become highly reflective, the specimens were coated in-house with aluminum in a vacuum deposition chamber.

To assess reliably any results from the dynamic experiments a detailed understanding of material response of the composite system is necessary. A sequence of experiments was performed to determine the material properties of the particular graphite/epoxy system used in this study. The material was assumed to be transversely isotropic. Properties $E_{11}$, $\nu_{12}$ and $\mu_{12}$ (see Fig. 3 for definition of axis), Young's modulus, Poisson's ratio and shear modulus respectively, were measured by performing quasi-static tests in an MTS hydraulic loading machine. The remaining properties were evaluated in the manner described in Walter and Ravichandran[20] after measurement of the dilatational and shear-wave speeds through the thickness of the composite. Since the procedure of measuring the properties of our material closely follow the lines of Walter and Ravichandran[20] no further details will be given here. For a quasi-static strain rate of approximately $10^{-4}\,s^{-1}$ the measured material properties are shown in Table 1.

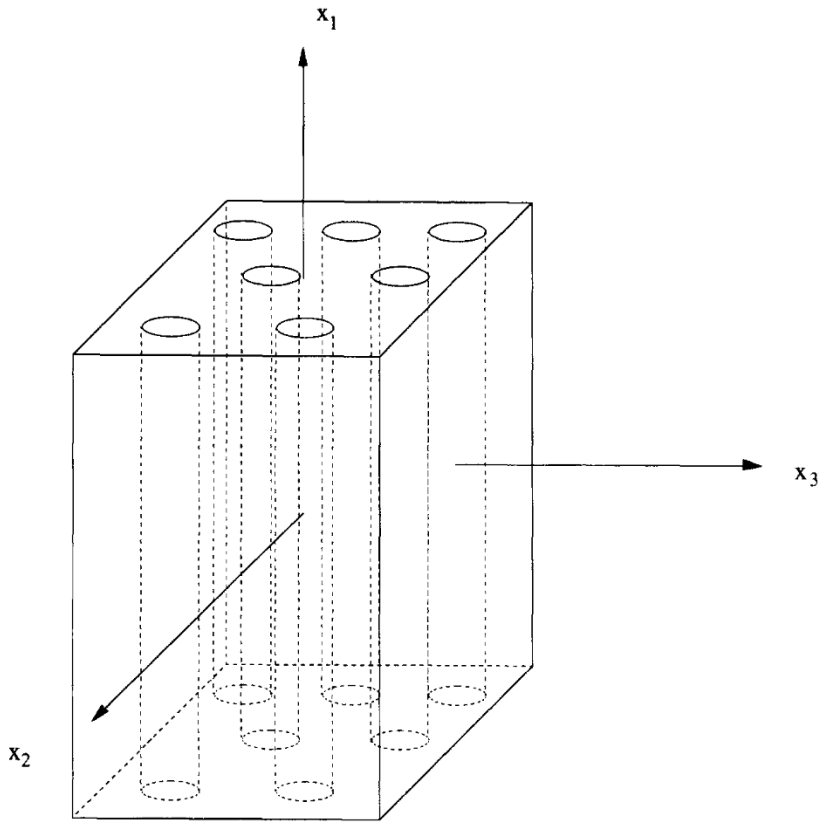


**Fig. 3.** Coordinate geometry of unidirectional composite specimen.

It is well known that certain polymer-matrix composites may exhibit significant strain-rate sensitivity over a range of loading rates (see, for example, Refs. 21–23). A preliminary study was therefore conducted to investigate the strain-rate sensitivity of our particular system. A split Hopkinson/Kolsky pressure-bar (SHKPB) apparatus was used to determine the variation of the material parameter $E_{11}$ over a range of strain rates. It is beyond the scope of the present paper to described in detail the SHKPB apparatus. For specific details of this apparatus the reader should refer to Kolsky.[24] The experimentally obtained variation of $E_{11}$ versus strain rate ($\dot{\varepsilon}$) is shown in Fig. 4. It can be seen that a significant rate sensitivity exists in this material, at least along the fiber direction. To fully characterize the material

**Table 1. Quasi-static elastic constants of the graphite/epoxy composite laminates used in this study**

| Stiffness properties | Compliance properties |
|---|---|
| $E_{11} = 150\,\text{GPa}$ | $b_{11} = \dfrac{1}{E_{11}} = 6{\cdot}66 \times 10^{-12}\,\text{Pa}$ |
| $E_{22} = E_{33} = 11{\cdot}6\,\text{GPa}$ | $b_{22} = b_{33} = \dfrac{1}{E_{22}} = \dfrac{1}{E_{33}} = 8{\cdot}64 \times 10^{-11}\,\text{Pa}$ |
| $\nu_{12} = \nu_{13} = 0{\cdot}36$ | $b_{12} = b_{21} = -\dfrac{\nu_{21}}{E_{22}} = -\dfrac{\nu_{12}}{E_{11}} = -2{\cdot}4 \times 10^{-12}\,\text{Pa}$ |
| $\nu_{23} = 0{\cdot}187$ | $b_{13} = b_{31} = -\dfrac{\nu_{13}}{E_{11}} = -\dfrac{\nu_{31}}{E_{33}} = -2{\cdot}4 \times 10^{-12}\,\text{Pa}$ |
| $\mu_{12} = 3{\cdot}5\,\text{GPa}$ | $b_{32} = b_{23} = -\dfrac{\nu_{23}}{E_{22}} = -\dfrac{\nu_{32}}{E_{33}} = -1{\cdot}61 \times 10^{-11}\,\text{Pa}$ |
| | $b_{66} = \dfrac{1}{\mu_{12}} = 2{\cdot}86 \times 10^{-10}\,\text{Pa}$ |

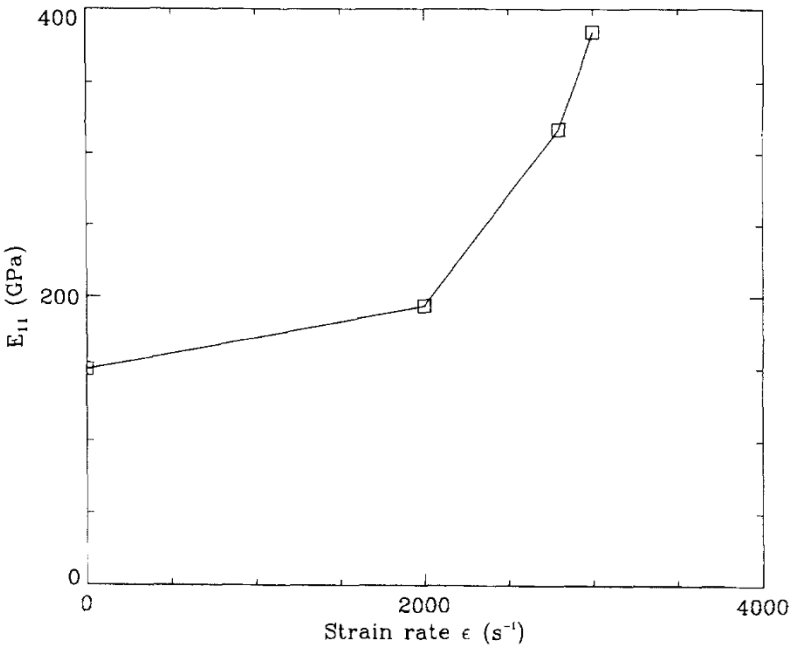


**Fig. 4.** Variation of $E_{11}$ versus strain rate ($\dot{\epsilon}$).

behavior one needs to perform similar measurements for all the independent elastic constants. As this is a preliminary study on dynamic fracture initiation in composites, an attempt to fully characterize the material was not made. When analysing the experimental results we, knowingly, made use of the quasi-static values of material properties quoted in Table 1. In a subsequent section we will investigate the validity of our assumption and estimate the error it introduces in the numerical results.

### 2.3 Experimental set-up and procedure

A symmetric one-point bend loading configuration was used to generate dynamic crack initiation and growth in our composite system. Each composite plate was loaded by means of a drop-weight tower. In all cases the impact speed used was $4\,m\,s^{-1}$. A schematic of the experimental set-up is shown in Fig. 1. Impact occurs on the top surface of the plate. Stress waves traveling down the width of the specimen and reflecting from the boundaries arrive at the notch or crack tip. Because of material anisotropy, these stress waves travel at different speeds in different directions. In addition, in a certain direction, e.g. along the fibers, the dispersive nature of wave propagation in the material causes a lengthening of the loading pulse. In any event, after some time a dynamic crack runs between fibers across the specimen width. As the time of crack initiation is around 25 $\mu$s after impact, the effects of dispersion are not very important since the length of the applied stress pulse, even in its undispersed form, is very long (around 120 $\mu$s) compared with the time of crack initiation. Loading is therefore continually applied throughout the whole event.

In all cases it was observed that fracture occurred in between the fibers (mostly along the fiber/matrix interface) and the crack propagated straight across the width of the specimen. The time-varying deformation fields surrounding the initially stationary and subsequently propagating crack tip produce a changing out-of-plane deformation on the surface of the composite plate. The reflection CGS technique in conjunction with high-speed photography was used to record in real time the slopes of the out-of-plane deformation field of the front surface. The light source used for specimen illumination was a Spectra-Physics argon-ion pulse laser (model 166-09). Two fine diffraction gratings (40 lines/mm) were used to provide optical differencing of the resultant distorted beam. A rotating-mirror high-speed camera (Cordin model 330A) was used for imaging. It is capable of running at framing rates of up to $2 \times 10^6$ frames $s^{-1}$. In the current tests the camera was operated at a framing rate of 590 000 frames $s^{-1}$ (i.e. 1·7 $\mu$s/frame). By using short laser pulses of 30 ns duration we were able to freeze the fast-changing deformation and thus produce sharp interference patterns. The laser pulsing was triggered by a strain gage on the specimen that sensed the impact of the drop-weight-tower hammer. The strain gage signal controls the start of the experiment completely.

## 3 OBSERVATIONS AND RESULTS

### 3.1 Crack tip speed

Figure 5 contains a selected sequence of CGS interferograms depicting dynamic crack growth in a unidirectional fiber-reinforced graphite/epoxy composite system. Crack propagation is parallel to the

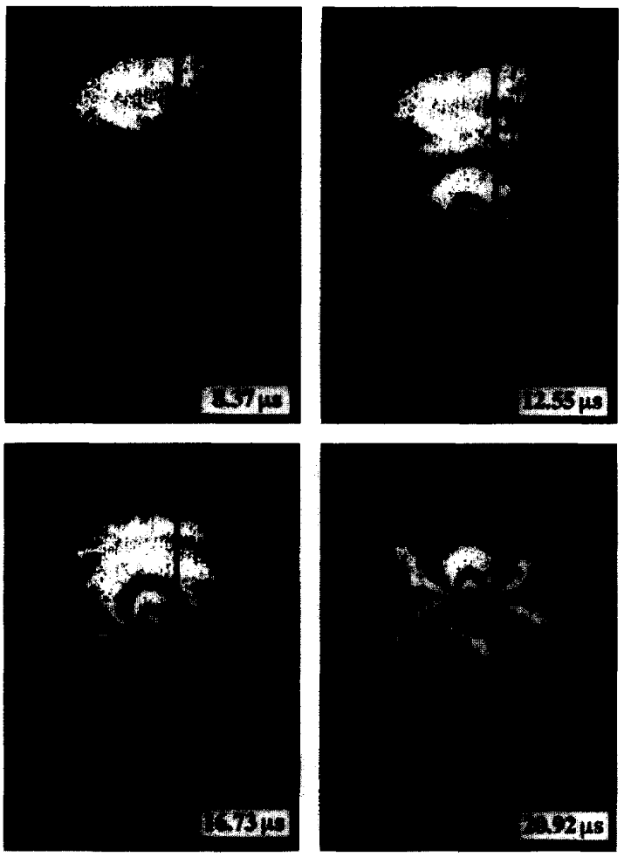

**Fig. 5.** Selected sequence of interferograms depicting dynamic crack growth in a unidirectional fiber-reinforced graphite/epoxy composite plate. Propagation is in the fiber direction.

fiber direction (along the vertical direction in Fig. 5). Time $t = 0\ \mu s$ is used to denote crack tip initiation. Thus negative times correspond to pre-initiation interferograms. For the experiment shown in Fig. 5 a 76 mm × 152 mm (3 in × 6 in) plate containing a blunt starter notch was used. Impact occurred at around $t = -24\ \mu s$. Also of interest is the travel time of a dilatational wave to propagate the width of the specimen, reflect from the free end and reach the stationary notch tip. Considering a wave speed (ignoring dispersion) in the fiber direction of $10\,000\ m\ s^{-1}$, this transit time is around $9\ \mu s$. The formation of interference fringes seen in Fig. 5 is governed by eqn (2). Therefore each fringe represents a constant value of the difference of out-of-plane displacement $u_3$ in the $x_1$ direction (the direction of shearing in this particular experiment). All fringes converge at the crack tip location. It is clearly seen that the crack tip location moves with time, indicating crack growth. By measuring the variation of crack tip position with time is possible to obtain crack tip speed, $v$. For the specimen shown in Fig. 5 (which had in-plane dimensions 76 mm × 152 mm (3 in × 6 in)) the crack tip speed history can be seen in Fig. 6. Positive time values denote events after crack initiation. (Clearly, for negative times, $v = 0\ m\ s^{-1}$.) The crack tip accelerates from about $700\ m\ s^{-1}$ at initiation to around $900\ m\ s^{-1}$ in a short time. However, it decelerates to less than $500\ m\ s^{-1}$ in under $40\ \mu s$ after initiation. It is believed that this deceleration is because of the fact that the growing crack tip enters a region of high compressive stresses as it approaches the loading area.

The crack tip speed history for an experiment on a 102 mm × 152 mm (4 in × 6 in) specimen is shown in Fig. 7. In this specimen a sharp precrack was introduced using a razor blade. It can be seen from

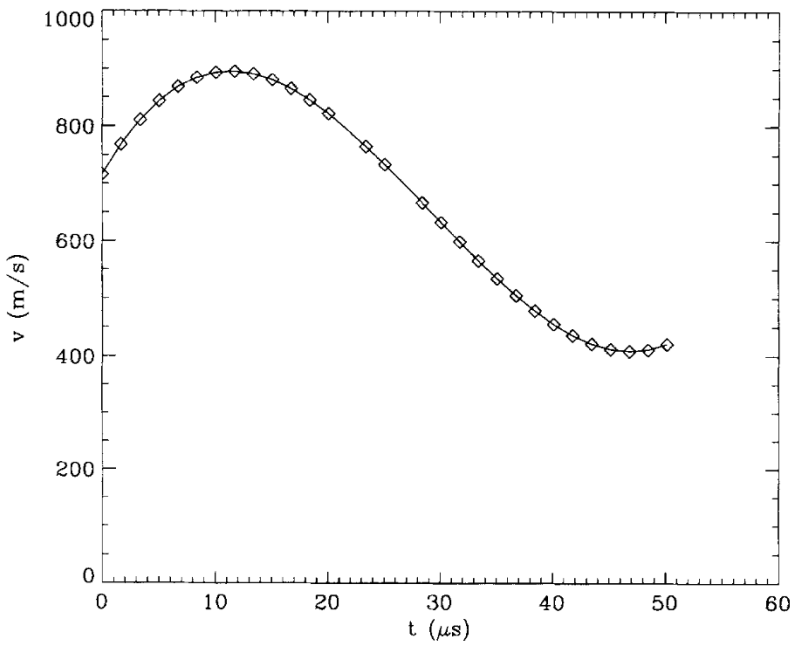


**Fig. 6.** Crack tip speed history in a 76 mm × 152 mm (3 in × 6 in) unidirectional graphite/epoxy composite plate containing a blunt starter crack.

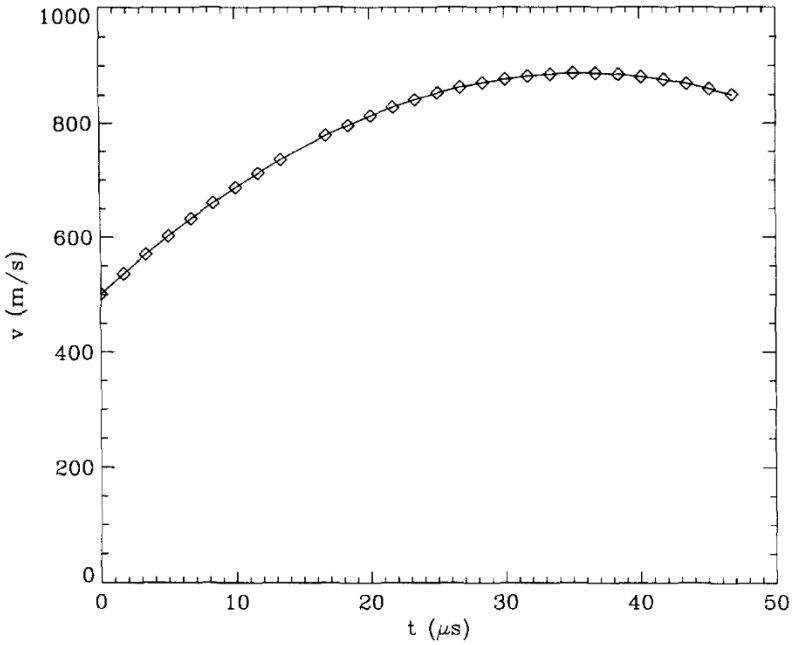


**Fig. 7.** Crack tip speed history in a 102 mm × 152 mm (4 in × 6 in) unidirectional graphite/epoxy composite plate containing a sharp starter crack.

Fig. 7 that in this case the crack tip speed starts at a lower value than in the previous experiment, around 500 m s$^{-1}$. This is expected since the sharp crack used here would store less energy before initiation than the wide notch used in the experiment of Fig. 5. In addition, and for the same reason, a longer acceleration time is necessary to reach 900 m s$^{-1}$. However, the speed remains constant at 900 m s$^{-1}$ in our time window of observation. This is a direct consequence of the fact that the loading point is now 25 mm (1 in) further away from the near-tip region than in the previous experiment.

In Fig. 5 we can clearly see the propagation of discrete stress waves that have been emitted by the growing crack as energy is released. Such waves have been observed in the past during highly dynamic crack growth in steels and other materials.[15] However in this case, unlike in homogeneous materials, the emitted wavefront is not circular. Figure 5 shows a distorted, almost elliptical, wave front traveling in the composite. This is a direct consequence of the anisotropy of the composite material. The wave speed along the fiber direction is much larger than along any other direction, thus leading to an elongation of the emitted wave along the fibers. The presence of emitted stress waves suggests a highly dynamic crack growth event. It is unknown at this point what the terminal crack growth speed for our graphite/epoxy system is. However it is believed that higher growth speeds will be achieved when the loading rate is increased.

A quantitative analysis of the interferograms shown in Fig. 5 is possible by utilization of the asymptotic crack tip fields obtained by Khanna and Shukla.[9] In the interest of brevity it is the aim of the present paper to describe only qualitative features about the dynamic crack growth portion of our experiments while concentrating primarily on measurements of *initiation* fracture toughness. The propagation part of the experiments are currently being analysed and will be discussed in a subsequent publication.

### 3.2 Dynamic initiation fracture toughness

Several authors have obtained the asymptotic nature of the stress and displacement fields surrounding the tip of a crack in a transversely isotropic medium subjected to quasi-static far-field loading.[25,26] Recently Liu *et al.*[4] provided explicit expressions for the near-tip out-of-plane displacement field surrounding such a crack. Their results are suitable for use in interpretation of CGS fringes using eqn (2). The out-of-plane displacement field for the case of symmetric loading derived by Liu *et al.*[4] is given by:

$$u_3 = \frac{hK_I}{2\sqrt{2\pi}}\left\{\frac{\mu_2(-b_{31}\mu_1^2+b_{32})}{(\mu_2-\mu_1)\sqrt{r_1}}\cos\frac{\theta_1}{2} - \frac{\mu_1(-b_{31}\mu_2^2+b_{32})}{(\mu_2-\mu_1)\sqrt{r_2}}\cos\frac{\theta_2}{2}\right\} \quad (3)$$

In eqn (3), $h$ is the plate thickness, $K_I$ is the mode-I stress-intensity factor, $r_\alpha = \sqrt{x_1^2 + \mu_\alpha x_2^2}$ and $\theta_\alpha = \tan^{-1}(\mu_\alpha x_2/x_1)$ with $x_1$, $x_2$ Cartesian coordinates centered between the two apparent crack tips (see Fig. 2). Quantities $\mu_\alpha$ depend upon material properties in a complicated fashion as derived in Liu *et al.*[4] The

values $b_{ij}$ are the elastic compliances of the material and are related to the elastic stiffnesses measured in Secton 2.2. These relationships, as well as their numerical values, are shown in Table 1 along with the measured elastic stiffnesses.

The combination of eqns (2) and (3) can be used to analyse quantitatively pre-initiation interferograms obtained in our experiments. (Analysis of propagation interferograms is possible only if eqn (3) is substituted with the equivalent expression for a dynamically growing crack.) A difference approach is used to analyse the experimental results. Since the diffraction gratings produce a shearing and recombination of the laser beam, two distinct crack tips, at O′ and O″, will be visible in the final image (see Fig. 2). By substituting eqn (3) in eqn (2) and utilizing Cartesian to polar coordinate system transformations, the formation of interference fringes on the image plane in regions where the displacement field is well approximated by eqn (3) will be governed by:

$$u_3(r'', \theta'') - u_3(r', \theta') = \frac{hK_I}{2\sqrt{2\pi}}\left\{\frac{\mu_2(-b_{31}\mu_1^2 + b_{32})}{(\mu_2 - \mu_1)\sqrt{r_1''}}\cos\frac{\theta_1''}{2} - \frac{\mu_1(-b_{31}\mu_2^2 + b_{32})}{(\mu_2 - \mu_1)\sqrt{r_2''}}\cos\frac{\theta_2''}{2}\right\} - \frac{hK_I}{2\sqrt{2\pi}} \times \left\{\frac{\mu_2(-b_{31}\mu_1^2 + b_{32})}{(\mu_2 - \mu_1)\sqrt{r_1'}}\cos\frac{\theta_1'}{2} - \frac{\mu_1(-b_{31}\mu_2^2 + b_{32})}{(\mu_2 - \mu_1)\sqrt{r_2'}}\cos\frac{\theta_2'}{2}\right\} = \frac{kp\varepsilon}{2\Delta} \quad (4)$$

A region on the specimen in which the most singular term of the asymptotic expansion for stresses and displacements (eqn (3)) well describes the actual stress and displacement field is called a $K$-dominant region. If experimental data of $x_1$, $x_2$ and $n$ are taken from interferograms exhibiting such a $K$-dominant region then extraction of $K_I$ is possible by performing a least-squares fitting procedure of eqn (4) to the experimental data. Note that in eqn (4) the primed and double primed coordinate systems are centered at the two apparent crack tips (Fig. 2).

When analysing all interferograms, data points lying directly ahead of the crack tip or within a circular region of $r/h < 0{\cdot}5$ ($h$: specimen thickness) were excluded. It is well known from studies in quasi-static and dynamic fracture of homogeneous materials[27,28] that a zone of three-dimensional deformation for homogeneous solids extends up to about $0{\cdot}5h$ away from the crack tip. In addition it has been seen that during dynamic fracture along a bimaterial interface a three-dimensional deformation zone extends ahead of the crack tip along the interface.[29] To the best of our knowledge, no results for the three-dimensional nature of the deformation surrounding the tip of a crack in an anisotropic medium exist at this point, although the authors are currently investigating this issue. As a first-order approximation, therefore, it was decided to use the largest possible three-dimensional zone (that of a bimaterial interface) in order to increase the chances of getting data from a region of two-dimensional plane stress.

The variation of the stress-intensity factor, $K_I$, with time for pre-initiation stages is shown in Fig. 8. Negative times correspond to instances before crack initiation, which is taken to occur at $t = 0\ \mu s$. The results shown in Fig. 8 are for the case of a 76 mm × 152 mm (3 in × 6 in) specimen containing a blunt starter notch. For this experiment impact occurred at around $t = -24\ \mu s$. The stress-intensity factor is seen to increase progressively towards its value at initiation. This increase occurs as more and more stress waves continually arrive at the crack tip. At a value of $K_{IC} = 2{\cdot}31\ MPa\,m^{1/2}$ crack initiation occurs. For the case of a sharp starter crack a similar variation in $K_I$ was seen. The measured initiation stress-intensity factor in that case was $K_{IC} = 1{\cdot}66\ MPa\,m^{1/2}$, which as expected is lower. It is instructive to compare the values for mode-I dynamic intiation fracture toughness with those for crack intiation under quasi-static loading conditions. Unfortuantely, for the material system used in this study, mode-I quasi-static fracture toughness data are not available. However, in the work of Liu *et al.*[4] the mode-I quasi-static fracture toughness of a similar graphite-fiber-reinforced composite material system was measured at $K_{IC} = 1{\cdot}8\ MPa\,m^{1/2}$, a value that compares well with the present results.

### 3.3 Importance of material strain-rate sensitivity

In all results presented above the quasi-static values of material properties (seen in Table 1) have been used. However, as was seen in Fig. 4, the elastic constants of our particular material are definitely rate sensitive. It is for this reason that the actual numerical values for dynamic initiation fracture toughness quoted in the previous section must be critically evaluated. They are only meant to be characteristic rather than precise values of toughness. However, the trends seen in Fig. 8 and between the different experiments will be preserved even when utilizing different material properties.

It is possible to estimate the reliability of our measurements by evaluating the spatial distribution of the instantaneous strain rate in the vicinity of the crack tip at each time. In the interest of brevity this will be performed only for the interferogram corresponding to crack initiation in one experiment. A measure of the strain rate used will be the equivalent strain rate defined as:

$$\dot{\varepsilon}_e = \sqrt{\tfrac{2}{3}\dot{\varepsilon}_{ij}\dot{\varepsilon}_{ij}} \quad (5)$$

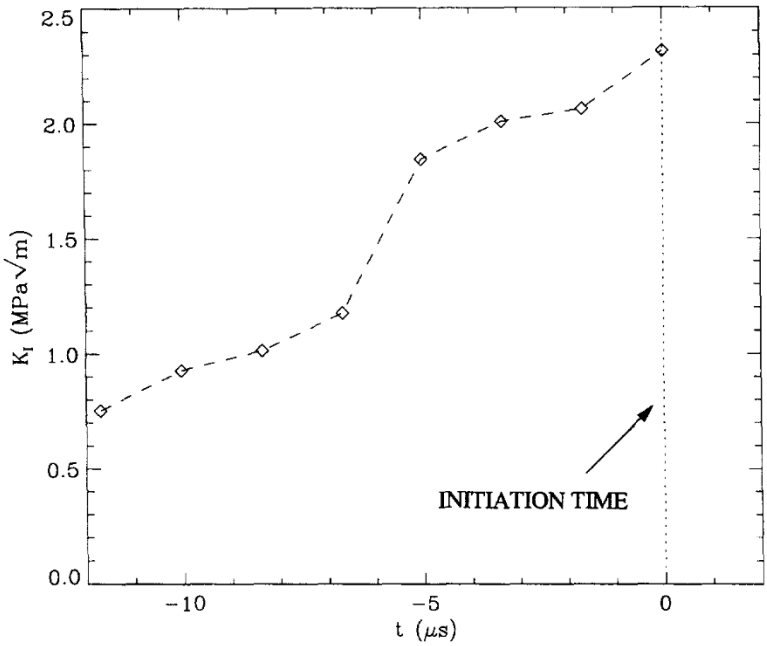


**Fig. 8.** Time history of dynamic stress-intensity factor for pre-initiation stages. Crack initiation occurs at $t = 0\ \mu s$.

From the work of Liu *et al.*[4] we can evaluate the through-thickness average strain rates by utilizing the rate of change of $K_I(t)$. A contour plot of the spatial distribution around the crack tip of equivalent strain (eqn (5)) at an instant corresponding to the initiation of crack extension, for the experiment shown in Fig. 8, is presented in Fig. 9. For this test the rate of change of $K_I(t)$ at intiation, sometimes defined as the loading rate, was $1{\cdot}3 \times 10^5$ MPa m$^{1/2}$ s$^{-1}$. It can be seen that the strain rate decreases to relatively low levels (less than $10^2$ s$^{-1}$) in the region from which experimental data is extracted to obtain the stress-intensity factor. However, it must be pointed out that the contour plot of eqn (5) itself has utilized the quasi-static values of material parameters. The result therefore represents an inclusion test, i.e. we can determine the minimum radius outside of which strain-rate effects *can* be neglected. It is therefore believed that the effect of the variation of material properties through rate, though definitely present, will not substantially alter the

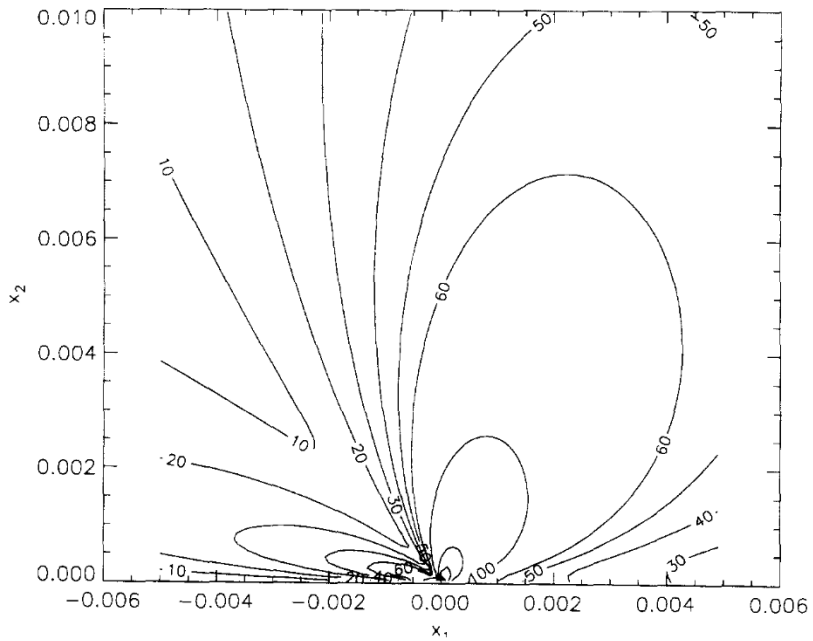


**Fig. 9.** Contour plot of strain-rate variation at the instant of crack initiation, $t = 0\ \mu s$, for the experiment shown in Fig. 8. Loading rate $\dot{K}_I = 1{\cdot}3 \times 10^5$ MPa m$^{1/2}$ s$^{-1}$.

fracture toughness measurements made from data points outside $r/h = 0{\cdot}5$.

## 4 CONCLUSIONS

In this paper we have demonstrated that it is possible to use the optical method of CGS in reflection to provide real-time imaging of dynamic fracture of composite plates. A one-point bend impact loading geometry was used to generate dynamic crack initiation and growth in unidirectional graphite/epoxy composite plates. Crack growth speeds up to 900 m s$^{-1}$ were measured and significant dynamic effects were observed through emission of stress waves from the propagating crack tip. Measurement of the dynamic initiation fracture toughness for our composite system was possible from the experimental interferograms. Fracture toughness was seen to depend on notch radius. This phenomenon has been observed in the past in homogeneous and bimaterial fracture. The measured fracture toughness quantities are close to typical values of fracture toughness of epoxies. This is to be expected because in the unidirectional lay-up crack initiation and growth occurs in the matrix material, avoiding fibers completely, since that is the weakest growth path.

## ACKNOWLEDGEMENTS

The support of ONR Grant N00014-90-J-1340 is gratefully appreciated. We would also like to acknowledge the help of Dr Mark Walter in conducting some of the material characterization of our composite.

## REFERENCES

1. Prahizar, S., Zachary, L. W. & Sun, C. T., Application of the principles of linear fracture mechanics to the composite materials. *Int. J. Fract.*, **20** (1982) 3–15.
2. Tohgo, K., Wang, A. S. & Chou, T. W., A criterion for splitting crack initiation in unidirectional fiber-reinforced composites. *J. Comp. Mater.*, **27** (1993) 1054–1076.
3. Binieda, W., Wang, A. S. D., Zhong, Y. & Reddy, E. S., A criterion for mixed-mode matrix cracking in graphite-epoxy composites. In *Composite Materials: Testing and Design*, ASTM STP 1059, ed. S. P. Garbo. American Society for Testing and Materials, Philadelphia, PA, 1990, pp. 287–300.
4. Liu, C., Rosakis, A. J., Stout, M. G. & Ellis, R., On the application of CGS interferometry to the study of cracks in fiber reinforced composites, *Int. J. Fract.* (submitted).
5. Tsai, Y. M., Dynamic behavior of an orthotropic material containing a central crack. *J. Pressure Vessel Technol.*, **111** (1989) 172–176.
6. Mannion, L. F. & Pipkin, A. C., Dynamic fracture of idealized fiber-reinforced materials. *J. Elasticity*, **13** (1983) 395–409.
7. Chiang, Y. J., Crack speed calculations for unidirectional laminae. *J. Comp. Technol. Res. (JCTRER)*, **13** (1991) 183–186.
8. Shukla, A. & Khanna, S. K., Effect of fiber reinforcement on dynamic crack growth in brittle matrix composites. *J. Engng Mater. Technol.*, **115** (1993) 140–145.
9. Khanna, S. K. & Shukla, A., Development of stress field equations and determination of stress intensity factor during dynamic fracture of orthotropic composite materials. *Engng Fract. Mech.*, **47** (1994) 345–359.
10. Chai, H., Knauss, W. G. & Babcock, C. D., Observation of damage growth in compressively loaded laminates. *Exp. Mech.*, **23** (1983) 329–337.
11. Chai, H. & Babcock, C. D., Two dimensional modelling of compressive failure in delaminated composites. *J. Comp. Mater.*, **19** (1985) 67–98.
12. Epstein, J. S., Deason, V. A. & Abdallah, M. G., Impact wave propagation in a thick composite plate using dynamic moiré interferometry. *Optics Lasers Engng*, **17** (1992) 35–46.
13. Zhu, G., Goldsmith, W. & Dharan, C. K. H., Penetration of laminated Kevlar by projectiles—I. Experimental investigation. *Int. J. Solids Struct.*, **29** (1992) 399–420.
14. Tippur, H. V., Krishnaswamy, S. & Rosakis, A. J., A coherent gradient sensor for crack tip measurements: Analysis and experimental results. *Int. J. Fract.*, **48** (1991) 193–204.
15. Rosakis, A. J., Two optical techniques sensitive to gradients of optical path difference: The method of caustics and the coherent gradient sensor (CGS). In *Experimental Techniques in Fracture*, ed. J. Epstein. VCH, New York, 1993, pp. 327–425.
16. Lee, Y. J., Lambros, J. & Rosakis, A. J., Analysis of coherent gradient sensing (CGS) by Fourier optics. *Optics Lasers Engng*, **25** (1996) 25–53.
17. Bruck, H. & Rosakis, A. J., On the sensitivity of coherent gradient sensing: I. A theoretical investigation of accuracy in fracture mechanics applications. *Optics Lasers Engng*, **17** (1992) 83–101.
18. Bruck, H. & Rosakis, A. J., On the sensitivity of coherent gradient sensing: II. An experimental investigation of accuracy in fracture mechanics applications. *Optics Lasers Engng*, **18** (1993) 25–51.
19. Tippur, H. K., Krishnaswamy, S. & Rosakis, A. J., Optical mapping of crack tip deformations using the method of transmission and reflection Coherent Gradient Sensing: A study of crack tip K-dominance. *Int. J. Fract.*, **52** (1991) 91–117.
20. Walter, M. E. & Ravichandran, G., An experimental investigation of damage evolution in a ceramic matrix composite. *J. Engng Mater. Technol.*, **117** (1995) 101–108.
21. Daniel, I. M., Hamilton, W. G. & LaBedz, R. H., Strain rate characterization of unidirectional graphite/epoxy composite. In *Composite Materials: Testing and Design*, ASTM STP 787, ed. I. M. Daniel. American Society for Testing and Materials, Philadelphia, PA, 1982, pp. 393–413.
22. Hollmann, K. & Hahn, H. T., Plane-strain fracture toughness of epoxies at different loading rates. *Polym. Engng Sci.*, **29** (1989) 523–530.
23. Pintado, P., Pedraza, C., del Castillo, J. M. & Benitez, F. G., Dynamic response of graphite–epoxy composite laminates under compression. In *Proc. 9th Int. Conf. on Composite Materials*, Madrid, Spain, 1993, pp. 438–444.
24. Kolsky, H., An investigation of the mechanical properties of materials at very high rates of loading. *Proc. Roy. Soc. Lond.*, **B62** (1949) 676–700.
25. Morris, D. H. & Hahn, H. T., Mixed-mode fracture of graphite/epoxy composites: Fracture strength. *J. Comp. Mater.*, **2** (1977) 124–138.

26. Tan, S. C., Mixed-mode fracture of notched composite laminates under uniaxial and multiaxial loading. *Engng Fract. Mech.*, **31** (1988) 733–746.
27. Rosakis, A. J. & Ravi-Chandar, K., On crack-tip stress states: An experimental evaluation of three dimensional effects. *Int. J. Solids Struct.*, **22** (1986) 121–134.
28. Krishnaswamy, S., Rosakis, A. J. & Ravichandran, G., On the extent of dominance of asymptotic elastodynamic crack-tip fields: II. Numerical investigation of three-dimensional and transient effects. *J. Appl. Mech.*, **58** (1991) 95–103.
29. Lee, Y. J. & Rosakis, A. J., Interfacial cracks in plates: A three dimensional numerical investigation. *Int. J. Solids Struct.*, **30** (1993) 3139–3158.